Acta Pharmaceutica Sinica B 2024;14(2):682–697

Chinese Pharmaceutical Association
Institute of Materia Medica, Chinese Academy of Medical Sciences

Acta Pharmaceutica Sinica B

www.elsevier.com/locate/apsb
www.sciencedirect.com

ORIGINAL ARTICLE

Targeting FAPα-positive lymph node metastatic tumor cells suppresses colorectal cancer metastasis

Shuran Fan[a,b,†], Ming Qi[a,b,e,†], Qi Qi[c,†], Qun Miao[a,b], Lijuan Deng[d], Jinghua Pan[e], Shenghui Qiu[e], Jiashuai He[e], Maohua Huang[a,b], Xiaobo Li[a,b], Jie Huang[a,b], Jiapeng Lin[b], Wenyu Lyu[b], Weiqing Deng[b], Yingyin He[b], Xuesong Liu[e], Lvfen Gao[e,*], Dongmei Zhang[a,b,*], Wencai Ye[a,b,*], Minfeng Chen[a,b,f,*]

[a]*State Key Laboratory of Bioactive Molecules and Druggability Assessment, Jinan University, Guangzhou 510632, China*
[b]*Guangdong Province Key Laboratory of Pharmacodynamic Constituents of Traditional Chinese Medicine and New Drugs Research, College of Pharmacy, Jinan University, Guangzhou 510632, China*
[c]*School of Medicine, Jinan University, Guangzhou 510632, China*
[d]*School of Traditional Chinese Medicine, Jinan University, Guangzhou 510630, China*
[e]*The First Affiliated Hospital of Jinan University, Guangzhou 510632, China*
[f]*State Key Laboratory of Chemical Oncogenomics, Guangdong Provincial Key Laboratory of Chemical Biology, Tsinghua Shenzhen International Graduate School, Shenzhen 518055, China*

Received 8 June 2023; received in revised form 18 September 2023; accepted 24 October 2023

KEY WORDS

Lymphatic metastasis;
Colorectal cancer;
Fibroblast activation protein α;
FAPα-activated prodrug;
Epithelial–mesenchymal

Abstract Lymphatic metastasis is the main metastatic route for colorectal cancer, which increases the risk of cancer recurrence and distant metastasis. The properties of the lymph node metastatic colorectal cancer (LNM-CRC) cells are poorly understood, and effective therapies are still lacking. Here, we found that hypoxia-induced fibroblast activation protein alpha (FAPα) expression in LNM-CRC cells. Gain- or loss-function experiments demonstrated that FAPα enhanced tumor cell migration, invasion, epithelial–mesenchymal transition, stemness, and lymphangiogenesis *via* activation of the STAT3 pathway. In addition, FAPα in tumor cells induced extracellular matrix remodeling and established an

*Corresponding authors.
E-mail addresses: minfengchen@jnu.edu.cn (Minfeng Chen), chywc@aliyun.com (Wencai Ye), dmzhang701@jnu.edu.cn (Dongmei Zhang), freshlucy07@126.com (Lvfen Gao).
[†]These authors made equal contributions to this work.
Peer review under the responsibility of Chinese Pharmaceutical Association and Institute of Materia Medica, Chinese Academy of Medical Sciences.

https://doi.org/10.1016/j.apsb.2023.11.002

transition;
STAT3;
Extracellular matrix remodeling;
Immunosuppressive

immunosuppressive environment *via* recruiting regulatory T cells, to promote colorectal cancer lymph node metastasis (CRCLNM). Z-GP-DAVLBH, a FAPα-activated prodrug, inhibited CRCLNM by targeting FAPα-positive LNM-CRC cells. Our study highlights the role of FAPα in tumor cells in CRCLNM and provides a potential therapeutic target and promising strategy for CRCLNM.

1. Introduction

Colorectal cancer (CRC) is the third most common malignant tumor with high incidence and mortality, and metastasis is the major cause of death in patients with CRC[1]. Lymph nodes (LN) are the first location for the spread and growth of metastatic CRC, which provides a gateway for distant metastasis[2]. Currently, surgical resection is the primary therapeutic strategy for patients with lymphatic metastasis. Nevertheless, owing to nodal skip metastasis and insidious metastasis, the efficacy of surgical resection for eliminating the metastatic LN is limited, resulting in patients with poor prognoses[3,4]. Therefore, identifying new targets and developing effective therapeutic strategies for the eradication of metastatic LN are of important clinical significance.

During the formation of the LN metastatic niche, metastatic cancer cells serve as one of the major components that promote tumor progression by acquiring epithelial-to-mesenchymal transition (EMT) and stemness phenotypes, inducing lymphangiogenesis, remodeling the extracellular matrix (ECM), and promoting immune suppression[5–7]. At the early stage of lymphatic metastasis, metastatic cancer cells in primary tumors acquire EMT and stemness properties to gain access to lymphatic vessels[8,9]. Meanwhile, metastatic cancer cells-derived secreted factors, including vascular endothelial growth factor, platelet-derived growth factor, fibroblast growth factor, hepatocyte growth factor, and angiopoietin-2, stimulate tumor lymphangiogenesis and the proliferation, migration, invasion and tube formation of human lymphatic endothelial cells (hLECs), which in turn secrete diverse chemokines to activate chemokine receptors on metastatic tumor cells[7,10], promoting the invasion of tumor cells into LN through lymphatic vessels in a positive feedback loop. At the stage of LN colonization, metastatic cancer cells modify collagen I, a major ECM component in the reorganized or pre-metastatic LN niche, leading to ECM remodeling to facilitate the establishment of metastatic LN[6,11], which is different from the hematogenous metastasis mediated by the degradation of collagen IV in the basement membrane[12]. Moreover, metastatic cancer cells can also recruit immunosuppressive cells such as myeloid-derived suppressor cells, tumor-associated macrophages, and regulatory T cells (Treg cells) into LN, thus generating an immunosuppressive environment and facilitating the formation of metastatic LN[13,14]. Although the properties and complex molecular programs of metastatic cancer cells in regulating lymphatic metastasis have been extensively studied, specific molecules that can serve as druggable targets for LN metastatic cancer cells are still lacking[5,15,16]. Therefore, investigating the characteristics of LN metastatic cancer cells, discovering potential molecular targets, and developing effective therapeutic strategies for the eradication of metastatic LN is urgently required.

Fibroblast activation protein alpha (FAPα) is a type II serine protease belonging to the family of prolyl-specific serine proteases, which displays both exopeptidase and collagenase activities that can specifically degrade collagen I and cleave N-terminal benzyloxy carbonyl-blocked (Z-blocked) Gly-Pro (Z-GP) dipeptide-linked substrates[17]. Previous studies reveal that FAPα is specifically expressed in tumor stromal cells including fibroblasts, pericytes, mesenchymal stem cells, and macrophages, whereas recent studies demonstrate that FAPα is also expressed in epithelial tumor cells[18,19]. FAPα in tumor cells plays an important role in tumor development and metastasis by regulating tumor growth, invasion, and angiogenesis[20,21]. However, the prevalence and significance of FAPα in LN metastatic cancer cells and its potential contribution to lymphatic metastasis remain unknown.

Here, we found that tumor hypoxia induced FAPα expression in lymph node metastatic colorectal cancer (LNM-CRC) cells, which promoted the migration, invasion, EMT, and stemness of tumor cells and stimulated lymphangiogenesis *via* STAT3 signaling. Moreover, FAPα in tumor cells induced metastatic LN formation through type-I collagen-dependent ECM remodeling and immunosuppressive cell recruitment. Furthermore, a FAPα-activated prodrug, Z-GP-DAVLBH, synthesized by our lab[22–24], exhibited potent cytotoxicity in FAPα-positive LNM-CRC cells, effectively inhibiting colorectal cancer lymph node metastasis (CRCLNM).

2. Materials and methods

2.1. Human tissue specimens

Clinical and pathological staging was performed according to the tumor-node-metastasis classification of the International Union Against Cancer. A total of 100 clinical tumor samples including primary tumor tissues derived from Stages I and II CRC patients ($n = 20$), primary tumor tissues ($n = 20$) and LN metastatic tumor tissues ($n = 20$) derived from Stage III CRC patients, primary tumor tissues ($n = 20$) and liver metastatic tumor tissues ($n = 20$) derived from Stage IV CRC patients, were obtained from 60 CRC patients at the First Affiliated Hospital of Jinan University (Guangzhou, China) following the ethical guidelines of the Declaration of Helsinki, and written informed consents were obtained. Detailed information is summarized In Supporting Information Table S1.

2.2. Cell lines and cell culture

Human CRC cell lines SW480, SW620, HCT116, HT-29, LoVo, and DLD1 were purchased from the American Type Culture Collection (VA). The mouse colorectal carcinoma cell line (MC38) was purchased from the BeNa Culture Collection (Beijing, China). These cells were cultured in DMEM (Gibco, NY, USA) containing

10% FBS (ExCell Bio, Shanghai, China) and 1% penicillin–streptomycin (Gibco). hLECs were obtained from iCell (Shanghai, China) and cultured in an Endothelial Cell Medium (ScienCell, CA, USA, 1001). All cell lines were maintained in a humidified atmosphere containing 5% CO_2, authenticated by the STR Multi-Amplification Kit (Microreader™21 ID System), and tested negative for mycoplasma contamination using the TransDetect® PCR Mycoplasma Detection Kit (Transgen, Beijing, China, FM311-01). Cells used in the hypoxia experiments were incubated in a modular incubator chamber (Billups-Rothenberg, CA, USA) filled with 1% O_2, 5% CO_2 and 94% N_2 at 37 °C before testing.

2.3. Isolation and characterization of primary tumor cells

Primary tumor tissues and metastatic LN tissues were aseptically harvested from CRCLNM patients or HCT116 CRCLNM xenografts, cut into small pieces (~1 mm^3 in size), and digested with the tumor tissue dissociation kit (Miltenyi Biotec, Kolner, Germany, 130-108-339). Single-cell suspension of digested tissues was obtained using a GentleMACS™ tissue processor (Miltenyi Biotec). Primary CRC (P-CRC) cells, LNM-CRC cells, $HCT116^{P}$ and $HCT116^{LNM}$ cells were filtered with a 100 μm filter, collected with anti-CD326 microbeads (Miltenyi Biotec., 130-061-101), and characterized as positive for EpCAM (Biolegend, CA, USA, 369809) and CK19 (R&D, MN, USA, AF3506) with purity >95%, as determined by flow cytometry.

2.4. Cell transfection and infection

Lentiviruses were constructed by Genechem (Shanghai, China), and lentiviral infection was performed according to the manufacturer's instructions. P-CRC and MC38 cells stably expressing FAPα were obtained by infection of cells with lentivirus harboring the FAPα plasmid and the corresponding vector (GV367, Ubi-MCS-SV40-EGFP-IRES-puromycin). *FAP*-knockdown LNM-CRC cells were generated by infection of LNM-CRC cells with *FAP* shRNA lentivirus and the corresponding negative control (PTSB-U6-PGK-Fluor-2A-ARG, Tsingke, Beijing, China). The shFAP sequences are listed in Supporting Information Table S2. P-CRC-luc, MC38-luc and HCT116-luc cells were generated by infection with lentivirus harboring luciferase (GV260, Ubi-MCS-firefly luciferase-IRES-puromycin). Green fluorescent protein (GFP)-positive cells were generated by infection of P-CRC cells with lentivirus harboring GFP (GV492, Ubi-MCS-3FLAG-CBh-gcGFP-IRES-Puromycin). All cells were selected using puromycin (2 μg/mL, Gibco, A1113803) following lentivirus infection. SW480 cells were transfected with the pFLAG-*FAP*-overexpressing plasmid or vector using Lipofectamine™3000 (Invitrogen, CA, L3000150) according to the manufacturer's instruction. SW620 cells were transfected with siRNA targeting *FAP*, *VEGFC* or the negative control, and SW480 cells were transfected with siRNA targeting *HIF1A*, *STAT3* or the negative control (Genepharma, Shanghai, China) to construct FAPα-, VEGFC-, HIF-1α-, or STAT3-knockdown cells, respectively. The sequences of si*FAP*, si*VEGFC*, si*HIF1A* and si*STAT3* are listed in Supporting Information Table S3.

2.5. Animals

Male BALB/c nude mice and C57BL/6 mice (aged 4–6 weeks) were purchased from BesTest (Zhuhai, China) and housed in a specific pathogen-free facility. All animal experiments were approved by the Animal Ethics Committee of Jinan University and complied with the ARRIVE guidelines (https://www.nc3rs.org.uk/arrive-guidelines), and were conducted according to the National Institutes of Health Guide for the Care and Use of Laboratory Animals.

2.6. In vivo experiments

CRCLNM xenografts were constructed as previously described, with minor modifications[25]. P-CRC or HCT116 cells (1×10^7) suspended in 50 μL PBS (HyClone, UT) were injected into the cecum wall of BALB/c nude mice. For drug administration, mice were randomly divided into vehicle and treatment groups. Mice in the treatment group were intravenously (i.v.) injected with 2 mg/kg Z-GP-DAVLBH once every other day for 14 days, while those in the vehicle group received saline (Servicebio, Wuhan, China)[23]. The bioluminescence signals of the tumor-bearing mice were detected using an IVIS Lumina LT imaging system (PerkinElmer, MA, USA) after injection with D-luciferin (Yeasen, Shanghai, China). To investigate the role of FAPα *in vivo*, $P\text{-}CRC^{Vector}$, $P\text{-}CRC^{FAP}$, $LNM\text{-}CRC^{shNC}$ and $LNM\text{-}CRC^{shFAP}$ cells were injected into the cecum wall of BALB/c nude mice, whereas $MC38^{Vector}$ and $MC38^{FAP}$ cells were injected into the cecum wall of C57/BL6 mice to generate $MC38^{Vector}$ and $MC38^{FAP}$ allografts. At the end of the experiment, blood was collected from the heart punctures for serum analysis, and the primary tumors and lymphatic metastases were collected for further analysis.

2.7. Hematoxylin and Eosin staining (H&E), immunohistochemistry, Masson staining, and Sirius Red staining

Paraffin-embedded tissue blocks were sectioned (5 μm). For H&E staining, the tissue sections were stained according to standard procedures. For immunohistochemical, antigen retrieval, blocking and staining were performed on the sections. Sections were incubated with specific primary antibodies at 4 °C overnight, and then stained with HRP-conjugated secondary antibodies. Positive staining was visualized using the DAB staining kit (Servicebio, G1212). Detailed information on the primary and secondary antibodies is provided in Supporting Information Table S4. For Masson staining, tissue sections were stained with a Masson Trichrome Staining Kit (Solarbio, Beijing, China, G1343) according to the manufacturer's instructions. For Sirius Red staining, tissue sections were assayed with a Sirius Red staining kit (Servicebio, GB1018) according to the manufacturer's protocol. Images were acquired using an Olympus BX53 inverted epifluorescence microscope (Olympus, Tokyo, Japan) and analyzed using Image-Pro Plus 6.0.

2.8. Immunofluorescence analysis

Paraffin-embedded sections were deparaffinized, antigen-retrieved, permeabilized, blocked, and incubated with primary antibodies overnight at 4 °C. The tissue sections were then incubated with HRP-conjugated secondary antibodies and visualized with iF488-Tyramide or iF555-Tyramide using TSAPLus Fluorescence Kits (Servicebio, G1236). For immunofluorescence assay in cell lines, cells were plated on confocal dishes containing cultured medium for 24 h. The cells were fixed, permeabilized, incubated with the primary antibody, and then incubated with Alexa Fluor 488-conjugated secondary antibody (Invitrogen) or

Alexa Fluor 594-phalloidin (Thermo Scientific, MA, USA, A12381). Images were photographed using a Zeiss LSM 800 confocal microscope (Zeiss, Oberkochen, Germany) and blindly analyzed using Image-Pro Plus 6.0. FAPα^+ tumor cells ratio (%) was calculated according to Eq. (1):

FAPα^+ tumor cells ratio (%) = Counts of FAPα^+ tumor cells of the sample/Mean counts of FAPα^+ tumor cells of the control group × 100 (1)

Tumor cells were identified by EpCAM staining in the tumor tissue, and FAPα^+ tumor cells were FAPα^+ EpCAM$^+$ cells.

2.9. Fluorescent in situ hybridization assay

The RNA fluorescence in situ hybridization (FISH) assay was performed using the Fluorescent in situ Hybridization Kit (GenePharma) according to the manufacturer's instructions. Briefly, tissue sections were incubated with CY3 labeled *FAP* probe in hybridization buffer. Subsequently, they were stained with primary antibodies followed by incubated with Alexa-coupled secondary antibodies. Images were visualized with microscopy. The antibodies used are provided in Supporting Information Table S4, and probe sequences are listed in Supporting Information Table S5. *FAP*$^+$ tumor cells ratio (%) was calculated according to Eq. (2):

FAP$^+$ tumor cells ratio (%) = Counts of *FAP*$^+$ tumor cells of the sample/Mean counts of *FAP*$^+$ tumor cells of the control group × 100 (2)

Tumor cells were identified by EpCAM staining in the tumor tissue, and *FAP*$^+$ tumor cells were *FAP*$^+$ EpCAM$^+$ cells.

2.10. Western blot analysis

Western blotting was performed as previously described[23]. Briefly, cells were harvested and lysed with ice-cold RIPA lysis buffer (Servicebio, G2002). The Pierce™ BCA Protein Assay Kit (Thermo Scientific, 23225) was used to measure the protein concentration. The protein blots were then visualized using Pierce ECL Western Blotting Substrate (Thermo Scientific, 23132). The primary antibodies used are listed in Table S4.

2.11. Real-time quantitative PCR (RT-qPCR)

Total RNA was extracted using the E.Z.N.A.® Total RNA Kit I (Omega Bio-Tek, GA, USA, R6834), and reverse transcription of total RNA (2 μg) was performed using All-in-One cDNA Synthesis SuperMix (Genestar, Beijing, China, A233) according to the manufacturer's protocol. Quantitative PCR was performed using 2× SYBR Green qPCR Master Mix (Genestar, A301) in a LightCycler 480 system (Roche, CA, USA). The mRNA levels of the target gene were normalized to those of the endogenous *ACTB* gene and calculated using the $2^{-\Delta\Delta Ct}$ method. Primer sequences are listed in Supporting Information Table S6.

2.12. Cell proliferation assay

Cell proliferation was detected using Cell Counting Kit-8 (CCK-8; Targetmol, Shanghai, China, C0005). Cells (5×10^3 per well) suspended in 100 μL DMEM were plated in a 96-well plate and cultured in a 37 °C incubator overnight. Following treatment with different concentrations of Z-GP-DAVLBH for 24 h, CCK-8 was added to each well, and the absorbance was measured at 450 nm using a microplate reader (Tecan, Männedorf, Switzerland). Cell viability (%) was calculated according to Eq. (3):

Cell viability (%) = The absorbance value of the treatment group/The mean of absorbance value of the control group × 100 (3)

2.13. EdU proliferation assay

Cells (3×10^3 per well) were seeded in a 96-well plate and treated with different concentrations of Z-GP-DAVLBH or conditioned medium for 24 h. Cell proliferation was analyzed using an EdU cell proliferation kit (Beyotime, Shanghai, China, C0075) according to the manufacturer's instructions. The number of EdU$^+$ cells was calculated using Image J software. Proliferative activity (%) was calculated according to Eq. (4):

Proliferative activity (%) = The value of the sample/The mean value of the control group × 100 (4)

2.14. Cell scratch assay

Cells were seeded in the Culture-Insert (ibidi, Munich, Germany, 80369). Images at time zero and 24 h later were captured using the Axio Observer inverted fluorescence microscope (Zeiss) and analyzed using ImageJ software (ImageJ Software Inc., MD, USA). Wound healing (%) was calculated according to Eq. (5):

Wound healing (%) = The value of the sample/The mean value of the control group × 100 (5)

2.15. Tube formation assay

Diluted Matrigel (Corning, NY, USA, 356234) was pre-coated in a 96-well plate at 37 °C for 30 min. hLECs (3×10^4 cells per well) supplemented with different conditioned mediums were seeded in Matrigel-coated plates. After 4 h of incubation, the capillary-like tubes were photographed under an inverted microscope, and the number of tubes was quantified using ImageJ software.

2.16. Propidium iodide staining

Cells (3×10^3 cells/well) were seeded in a 96-well plate and treated with different concentrations of Z-GP-DAVLBH for 24 h. The cells were then stained with propidium iodide (PI, Beyotime, ST512), following the manufacturer's instructions. The number of

PI^+ cells was determined using ImageJ software. Apoptotic cells (%) were calculated according to Eq. (6):

Apoptotic cells (%) = The value of the sample/The mean value of the control group × 100 (6)

2.17. Cell migration and invasion assays

For the migration assay, cells (1×10^5 per well) suspended in serum-free DMEM were seeded in the upper chamber of a 24-well transwell with an 8 μm pore size membrane (Corning, 3422). For the invasion assay, cells were added to the upper chamber that was pre-coated with 40 μL of diluted Matrigel at 37 °C for 30 min. Different concentrations of Z-GP-DAVLBH or conditioned medium were added to the lower chamber. Following a certain period of incubation, the migrated/invaded cells were fixed with 4% paraformaldehyde (Servicebio), stained with 0.1% Crystal Violet dye (Sigma−Aldrich, MO, USA), and photographed using an Olympus BX53 inverted microscope (Olympus). Migrated/Invaded cells (%) were calculated according Eq. (7):

Migrated/Invaded cells (%) = The value of the sample/The mean value of the control group × 100 (7)

2.18. Sphere-forming assay

Cells (1×10^4 per well) with indicated treatments were labeled with PKH67 fluorescent dye using a PKH67 green fluorescent cell linker kit (Sigma−Aldrich) and seeded in an ultra-low attachment 96-well-plate (Corning, 7007) with DMEM-F12 (VivaCell, Shanghai, China) medium containing epidermal growth factor (20 ng/mL, PeproTech, NJ, USA, 100-47), fibroblast growth factor (20 ng/mL, PeproTech, 100-18B) and B-27 serum-free-supplement (Gibco, 17504-044) for 24 h. PKH67-positive spheres were imaged after culturing for 5 days using the Axio Observer inverted fluorescence microscope (Zeiss). Sphere forming efficiency (%) was calculated according to Eq. (8):

Sphere forming efficiency (%) = The fluorescence intensity value of the sample/The mean fluorescence intensity value of the control group × 100 (8)

2.19. Enzyme-linked immunosorbent assay (ELISA)

VEGFC ELISA Kits (Liankebio, Hangzhou, China), CCL17 and CCL22 ELISA Kits (Neobioscience, Shenzhen, China) were used to measure VEGFC, CCL17 and CCL22 levels in the cell cultural supernatant or serum according to the manufacturer's instructions.

2.20. Chromatin immunoprecipitation (ChIP)-qPCR assay

The ChIP assay was performed using the SimpleChIP™ Enzymatic Chromatin IP Kit (Cell Signaling Technology, 9002S) following the manufacturer's instructions. The antibodies used are shown in Table S4, and the primers used for ChIP-qPCR analysis are shown in Table S7. The standard formula used to evaluate the percentage of input was as Eq. (9):

$$\text{Input (\%)} = 2\% \times 2^{(\text{C[T]2\% input sample} - \text{C[T]IP sample})} \quad (9)$$

where C[T] stands for threshold cycle of PCR reaction.

2.21. Flow cytometry analysis

Metastatic LN tissues from $MC38^{Vector}$ and $MC38^{FAP}$ allografts were finely minced into small pieces and subjected to digestion with 1 mg/mL of type IV collagenase (Servicebio) and 200 U/mL of hyaluronidase (Servicebio) for 30 min at 37 °C. Following digestion, the dissociated tissue samples were then filtered through a 30-μm mesh filter, and the resultant cells were collected by centrifugation at 600 × *g* for 5 min. To identify mouse $CD4^+CD25^+FOXP3^+$ Treg cells, the cells were stained with anti-CD4-FITC, anti-CD25-APC and anti-FOXP3-PE antibodies using a mouse regulatory T cell staining kit (Liankebio). Then, the cells were acquired using a FACS Canto II flow cytometer (BD Biosciences, CA, USA) and the data were analyzed using FlowJo VX software (FlowJo LLC, OR).

2.22. Statistical analysis

All quantitative data are presented as mean ± standard error of the mean (SEM). Statistical analyses were performed using GraphPad Prism 8.0 (GraphPad Software, Inc., CA, USA). Statistical differences between two groups were evaluated using a two-tailed unpaired *t*-test, and differences among three or more groups were evaluated using one-way ANOVA followed by Tukey's *post hoc* test. Kaplan−Meier survival curves were constructed and analyzed using the log-rank test. $P < 0.05$ was considered to be statistically significant.

3. Results

3.1. Tumor cells expressing FAPα are associated with colorectal cancer lymph node metastasis

Firstly, the protein and gene expression levels of FAPα in tumor cells were evaluated in primary and metastatic tumor tissues derived from patients with CRC. Immunofluorescence staining and FISH assay showed that the protein and gene expression levels of FAPα in $EpCAM^+$ tumor cells were higher in LN metastatic tumor tissues than those in primary tumor tissues or liver metastatic tumor tissues (Fig. 1A). In CRC cell lines with microsatellite stability (SW620, SW480 and HT-29) and microsatellite instability (DLD1, HCT116 and LoVo), FAPα expression was significantly higher in the LN metastatic line SW620 compared to other cell lines (Supporting Information Fig. S1). To confirm the distinct expression of FAPα in LN metastatic tumor cells, P-CRC and LNM-CRC cells isolated from the primary or LN metastatic lesions in CRCLNM patients (Supporting Information Fig. S2A) were identified by flow cytometry and immunofluorescence staining (Fig. S2B and S2C). RT-qPCR and Western blotting showed that the expression levels of FAPα were higher in LNM-CRC cells than in P-CRC cells (Fig. 1B). Moreover, in the P-CRC cells-constructed patient-derived xenografts, FAPα expression in LN metastatic tumor tissues was higher than that in primary tumor tissues (Figs. 1C, D, and S2D). Consistently, another CRCLNM model was generated using HCT116 cells, and the expression of FAPα was found to be higher in $HCT116^{LNM}$ cells (derived from LN metastatic tumor tissues of HCT116 CRCLNM xenografts) compared to $HCT116^{P}$ cells (derived from primary tumor tissues of HCT116 CRCLNM xenografts) (Supporting Information Fig. S3). These data indicate that FAPα is highly expressed in

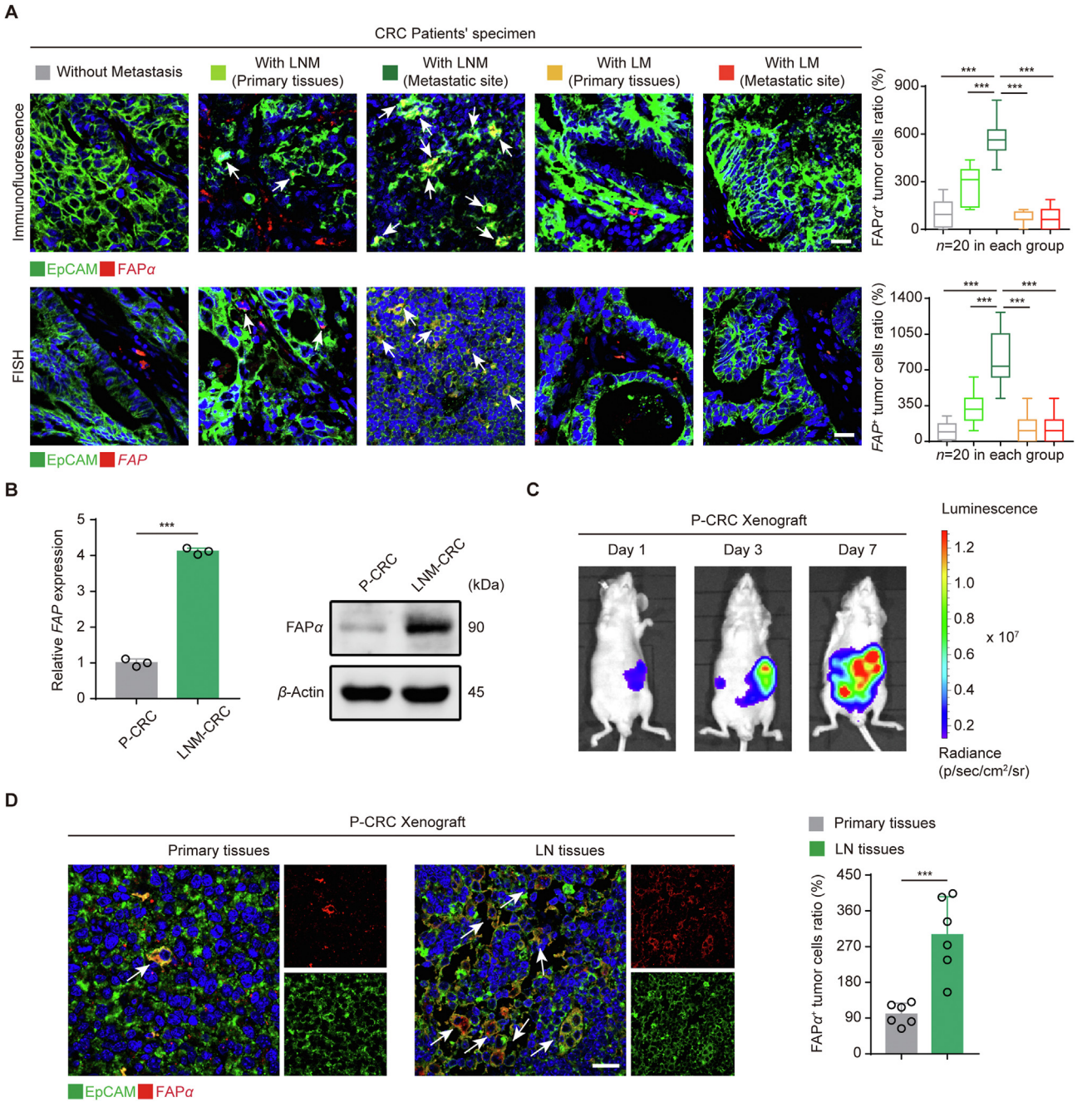

Figure 1 High expression of FAPα in tumor cells is associated with colorectal cancer lymph node metastasis. (A) Immunofluorescence and FISH analysis of the colocalization of EpCAM and FAPα or *FAP* in the primary and metastatic tissues derived from CRC patients. Representative images and quantification of the overlapping fluorescence of EpCAM and FAPα are shown ($n = 20$ in each group). White arrows indicate FAPα$^+$EpCAM$^+$ tumor cells. Scale bar, 20 μm. (B) RT-qPCR and Western blot analysis of FAPα expression in P-CRC and LNM-CRC cells ($n = 3$). P-CRC cells or LNM-CRC cells were isolated from the primary tumor tissues or the metastatic LN in a CRCLNM patient, respectively. (C) Bioluminescence imaging of growth and lymphatic metastasis of patient-derived CRCLNM xenografts ($n = 6$). (D) Immunofluorescence staining and quantification of FAPα$^+$ (red) EpCAM$^+$ (green) tumor cells in tumor tissues derived from patient-derived CRCLNM xenografts ($n = 6$). Scale bar, 20 μm. White arrows indicate FAPα$^+$ tumor cells. Data are presented as mean ± SEM. ***$P < 0.001$ (one-way ANOVA with Tukey's *post hoc* comparison in A, two-tailed unpaired *t*-test in B and D). CRC, colorectal cancer; LN, lymph node; LNM, lymph node metastasis; LNM-CRC, lymph node metastatic colorectal cancer; LM, liver metastasis; P-CRC, primary colorectal cancer.

LNM-CRC cells with either microsatellite stability or microsatellite instability.

We proceeded to investigate the underlying mechanism by which FAPα expression was induced in tumor cells. Given that hypoxia has been demonstrated to be involved in lymphatic metastasis *via* the HIF-1α pathway[26], we hypothesized that FAPα expression in tumor cells might be regulated by HIF-1α. Our results showed that the expression of HIF-1α was significantly increased in primary tumor tissues derived from CRCLNM patients compared to CRC patients without lymphatic

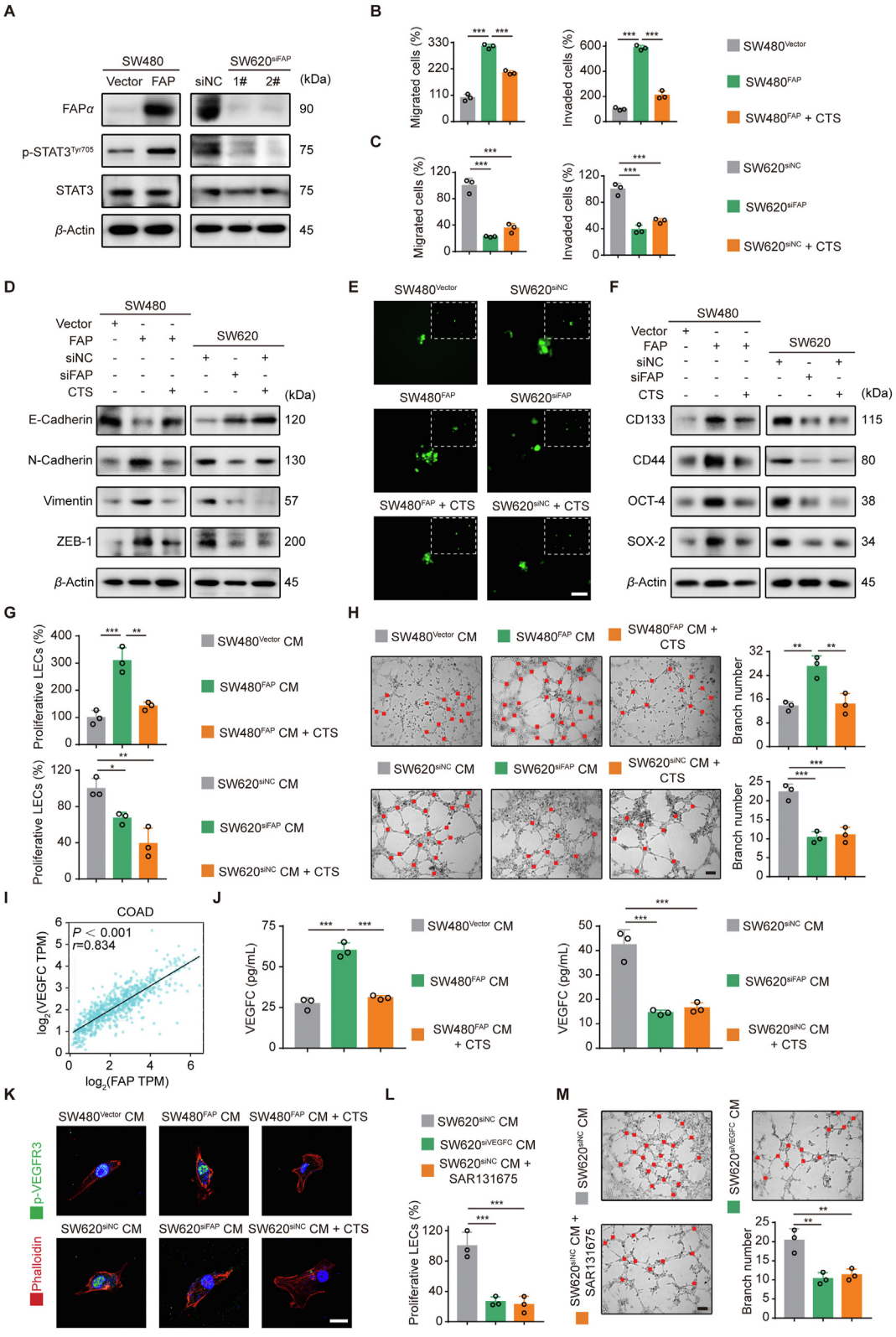

Figure 2 FAPα induces tumor cell migration, invasion, EMT, stemness, and lymphangiogenesis *via* the STAT3 pathway. (A) Western blot analysis of FAPα, STAT3, and p-STAT3 in SW480^{Vector}, SW480^{FAP}, SW620^{siNC} and SW620^{siFAP} cells (n = 3). (B) Quantification of migrated and invaded FAPα-overexpressing SW480 cells treated with or without CTS (n = 3). (C) Quantification of migrated and invaded FAPα-knockdown SW620 cells treated with or without CTS (n = 3). (D) Western blot analysis of E-cadherin, N-cadherin, Vimentin and ZEB-1 in FAPα-overexpressing SW480 cells or FAPα-knockdown SW620 cells treated with or without CTS (n = 3). (E) The sphere-forming assay of SW480 or SW620 cells in the absence or presence of CTS (n = 3). Original magnification: 20× (enlargement) and 10× (insert). Scale bar, 100 μm.

metastasis (Supporting Information Fig. S4A). Moreover, hypoxic significantly enhanced the expression of FAPα in SW480 cells by upregulating HIF-1α expression (Fig. S4B). In addition, overexpression of HIF-1α markedly increased the expression of FAPα in SW480 cells under normoxic conditions, whereas knockdown of HIF-1α decreased the expression of FAPα in SW480 cells under hypoxic conditions (Fig. S4C−S4F). However, the ChIP-qPCR assay showed that HIF-1α did not bind to the *FAP* promoter under hypoxic conditions (Fig. S4G), suggesting that hypoxia may induce FAPα expression in tumor cells through the HIF-1α pathway in a transcription-independent manner. Taken together, these data demonstrate that hypoxia induced FAPα expression in tumor cells may be associated with CRCLNM.

3.2. *FAPα promotes tumor cell motility, EMT, stemness, and lymphangiogenesis via activation of STAT3 in vitro*

We next investigated the role of FAPα in tumor cells in CRCLNM. SW480 cells (derived from primary tumor tissues) with intrinsically low expression of FAPα were transfected with a vector or FAPα plasmid to generate $SW480^{Vector}$ and $SW480^{FAP}$ cells, respectively. In parallel, SW620 cells (derived from LN metastatic tumor tissues) with intrinsically high expression of FAPα were transfected with negative control siRNA or *FAP* siRNA to generate $SW620^{siNC}$ or $SW620^{siFAP}$ cells, respectively (Fig. 2A, Supporting Information Fig. S5A). With these cells, downstream signaling of FAPα associated with tumor metastasis, such as STAT3, P65, AKT, β-catenin and ERK[21,27,28], were firstly examined. Our results showed that the phosphorylation levels of STAT3, P65, and AKT were significantly upregulated in $SW480^{FAP}$ cells compared to those in $SW480^{Vector}$ cells. Notably, among these factors, the phosphorylation levels of STAT3 exhibited the most significantly upregulated in CRC cells with higher FAPα expression, whereas they markedly reduced in FAPα-knockdown CRC cells (Figs. 2A, S5B). Functionally, overexpression of FAPα promoted migration, invasion and decreased the expression of the epithelial marker E-cadherin, and increased the expression of the mesenchymal markers Vimentin and N-cadherin in SW480 cells, while knockdown of FAPα showed the opposite effects in SW620 cells (Figs. 2B−D, S5C−S5E). Moreover, the levels of FAPα in tumor cells were positively correlated with spheroid size and increased expression of stemness markers including CD44, CD133, SOX2 and OCT4 in CRC cells (Figs. 2E, F, S5F). However, these effects were significantly attenuated by cryptotanshinone (CTS, a specific STAT3 inhibitor) (Figs. 2B−F, S5C−S5F). To further investigate whether STAT3 is a specific pathway through which FAPα promotes tumor metastasis, we constructed FAPα-overexpressing SW480 cells transfected with siNC ($SW480^{Vector}_{siNC}$, $SW480^{FAP}_{siNC}$) or siSTAT3 ($SW480^{Vector}_{siSTAT3}$, $SW480^{FAP}_{siSTAT3}$) (Supporting Information Fig. S6A and S6B). Data showed that migration, invasion, and the expressions of Vimentin, N-cadherin, and ZEB-1 were significantly increased, while the expression of E-cadherin was decreased in $SW480^{FAP}_{siNC}$ cells. However, these effects were reversed by the knockdown of STAT3 (Fig. S6C−S6E). Moreover, the sphero-forming ability and the expression of stemness markers, including CD133, CD44, SOX-2 and OCT-4, were significantly increased in $SW480^{FAP}_{siNC}$ cells, which were ameliorated by STAT3 knockdown (Fig. S6F−S6H).

Lymphangiogenesis is a crucial event for lymph node metastasis, in which the proliferation and tube formation of LECs are the basic processes[29]. Besides, it is also induced by STAT3 signaling in tumor progression[30]. Our results showed that the conditioned medium from CRC cells with high levels of FAPα ($SW480^{FAP}$ and $SW620^{siNC}$ cells) significantly promoted the proliferation and tube formation of hLECs, which was attenuated by CTS; whereas the conditioned medium from CRC cells with low expression of FAPα ($SW480^{Vector}$ and $SW620^{siFAP}$ cells) inhibited the proliferation and tube formation of hLECs (Fig. 2G, H, Supporting Information Fig. S7A). Vascular endothelial growth factor C (VEGFC) is a key regulator of lymphangiogenesis[31]. Correlation analysis using the Gene Expression Profiling Interactive Analysis database revealed a positive correlation between *FAP* and *VEGFC* expression in CRC patients (Fig. 2I). We next investigated the effect of FAPα on the expression and secretion of VEGFC in tumor cells. Data showed that the expression and secretion of VEGFC were elevated in CRC cells with higher expression of FAPα, while these effects were significantly attenuated by CTS (Figs. 2J, and S7B and S7C). In addition, our results showed that phosphorylation of VEGFR3 was notably increased in hLECs treated with conditioned medium from $SW480^{FAP}$ and $SW620^{shNC}$ cells compared to that in hLECs treated with the conditioned medium from $SW480^{Vector}$ and $SW620^{shFAP}$ cells, which was attenuated by CTS (Fig. 2K). In addition, proliferation and tube formation were significantly inhibited in hLECs treated with conditioned medium from VEGFC-knockdown SW620 cells ($SW620^{siVEGFC}$) compared to those in hLECs treated with conditioned medium from $SW620^{siNC}$ cells (Figs. 2L, M, and S7D). Furthermore, SAR131675 (a VEGFR3 specific inhibitor) treatment also attenuated the proliferation and tube formation of hLECs treated with $SW620^{siNC}$ medium (Figs. 2L, M, and S7D). Taken together, these data indicate that FAPα induces migration, invasion, EMT and stemness in tumor cells, and stimulates lymphangiogenesis *via* activation of STAT3 signaling.

(F) Western blot analysis of CD133, CD44, OCT-4 and SOX-2 expression in SW480 or SW620 cells in the absence or presence of CTS ($n = 3$). (G) Quantification of EdU^+ hLECs treated with conditioned medium from SW480 or SW620 cells in the absence or presence of CTS ($n = 3$). (H) Tube formation by hLECs treated with conditioned medium from SW480 or SW620 cells in the absence or presence of CTS ($n = 3$). Scale bar, 100 μm. (I) Correlation analysis of *FAP* and *VEGFC* expression in patients with CRC using the Gene Expression Profiling Interactive Analysis database (http://gepia.cancer-pku.cn/). (J) ELISA analysis of VEGFC in hLECs treated with conditioned medium from SW480 or SW620 cells in the absence or presence of CTS ($n = 3$). (K) Immunofluorescence staining of p-VEGFR3 in hLECs treated with conditioned medium from SW480 or SW620 cells in the absence or presence of CTS ($n = 3$). Scale bar, 20 μm. (L) Quantification of EdU^+ hLECs treated with conditioned medium from SW620 cells in the absence or presence of SAR131675 ($n = 3$). (M) Tube formation of hLECs treated with conditioned medium from SW620 cells in the absence or presence of SAR131675 ($n = 3$). Scale bar, 100 μm. Data are presented as mean ± SEM. $^*P < 0.05$, $^{**}P < 0.01$, $^{***}P < 0.001$ by one-way ANOVA with Tukey's *post hoc* comparison. CTS, cryptotanshinone.

3.3. FAPα promotes colorectal cancer lymph node metastasis in vivo

To further investigate the effect of FAPα in tumor cells in CRCLNM *in vivo*, P-CRC cells with intrinsically low expression of FAPα were infected with lentivirus-containing vector or FAPα overexpression plasmid to generate P-CRC^{Vector} or FAPα-overexpressing P-CRC^{FAP} cells, respectively. In parallel, LNM-CRC cells with intrinsically high levels of FAPα were infected with lentiviruses harboring negative control shRNA or *FAP* shRNA to generate LNM-CRC^{shNC} or FAPα-knockdown LNM-CRC^{shFAP} cells (Supporting Information Fig. S8). CRCLNM xenografts were constructed using these cell lines. Data showed that overexpression of FAPα in tumor cells stimulated lymphatic metastasis whereas FAPα knockdown exerted the opposite effects, as indicated by the increased number of LN metastatic nodules in P-CRC^{FAP} and LNM-CRC^{shNC} xenografts compared with those in P-CRC^{Vector} and LNM-CRC^{shFAP} xenografts, respectively (Fig. 3A, B). Consistently, the EMT and stemness in P-CRC^{FAP} and LNM-CRC^{shNC} xenografts were more prominent than those in P-CRC^{Vector} and LNM-CRC^{shFAP} xenografts, as evidenced by the decreased expression of E-cadherin, and increased expression of Vimentin, CD44, and CD133 (Fig. 3C). Furthermore, the expression of VEGFC and the numbers of lymphatic vessels in the P-CRC^{FAP} and LNM-CRC^{shNC} xenografts were higher than those in the P-CRC^{Vector} and LNM-CRC^{shFAP} xenografts (Fig. 3C, D). Taken together, these data suggest that FAPα promotes tumor cell EMT, stemness and lymphangiogenesis, thus facilitating CRCLNM.

3.4. FAPα regulates ECM remodeling and induces an immunosuppressive environment in metastatic lymph nodes

ECM remodeling plays a critical role in lymphatic metastasis[12]. Type I collagen is the main ECM component in LN, and ECM remodeling is characterized by collagen I deposition and linearization[6,11,32,33]. Hence, we further investigated whether FAPα can remodel the ECM in LN by modulating collagen fiber deposition and linearization through its collagen I-specific gelatinase activity, which promotes the formation of a permissive microenvironment to facilitate lymphatic metastasis. Our results showed that P-CRC^{FAP} and LNM-CRC^{shNC} xenografts displayed increased collagen fiber deposition in the metastatic LN compared to the P-CRC^{Vector} and LNM-CRC^{shFAP} xenografts (Fig. 4A). Moreover, immunofluorescence staining revealed that collagen I was arranged irregularly with curly and unfixed outlines in P-CRC^{Vector} and LNM-CRC^{shFAP} xenografts, whereas it was arranged tightly with parallel orientation in P-CRC^{FAP} and LNM-CRC^{shNC} xenografts (Fig. 4B). Treg cell-mediated immunosuppression is one of the most crucial tumor immune evasion mechanisms for the formation of pre-metastatic LN niche[13]. Our results showed that the expression of Treg cell recruitment-related factors was increased in CRC cells with high expression of FAPα (SW480^{FAP} and P-CRC^{FAP} cells), and the secretion of CCL17 and CCL22 was upregulated in the conditioned medium from FAPα-overexpressing CRC cells (Fig. 4C, D). Murine colon adenocarcinoma cell line MC38 was infected with lentivirus-containing vector or FAPα overexpression plasmid to construct MC38^{Vector} and MC38^{FAP} cells, which were injected into the cecum wall of C57/BL6 mice to generate MC38^{Vector} and MC38^{FAP} allografts, respectively (Fig. 4E). ELISA assay showed that the serum levels of CCL22 were higher in MC38^{FAP} allografts than in MC38^{Vector} allografts (Fig. 4F). The number of $CD4^{+}FOXP3^{+}$ Treg cells in metastatic LN was increased in MC38^{FAP} allografts compared to that in MC38^{Vector} allografts (Fig. 4G, H). Taken together, these data indicate that FAPα in tumor cells regulates ECM remodeling and establishes an immunosuppressive microenvironment to facilitate the formation of the metastatic LN niche.

3.5. Z-GP-DAVLBH inhibits proliferation, induces apoptosis, and inhibits the migration, invasion, EMT, and stemness of lymph node metastatic tumor cells

We further investigated whether targeting FAPα-positive LN metastatic tumor cells could effectively inhibit CRCLNM. Our results showed that Z-GP-DAVLBH significantly decreased the viability and proliferation of LNM-CRC, SW620 and HCT116^{LNM} cells in a concentration-dependent manner (Supporting Information Fig. S9). PI staining and Western blotting showed that Z-GP-DAVLBH treatment markedly induced apoptosis of LN metastatic tumor cells in a dose-dependent manner (Fig. 5A, B, Supporting Information Fig. S10). In addition, Z-GP-DAVLBH treatment significantly inhibited the migration and invasion of LN metastatic tumor cells in a dose-dependent manner (Fig. 5C, D, Supporting Information Fig. S11A and S11B), which might be a result of its inhibitory effect on EMT, as indicated by the increased expression of E-cadherin and decreased expression of N-cadherin, Vimentin and ZEB1 in the LN metastatic tumor cells (Figs. 5E, S11C). Moreover, Z-GP-DAVLBH significantly decreased the expression of stemness markers including CD133, CD44, SOX-2 and OCT-4 in LN metastatic tumor cells (Figs. 5F, S11D). The sphero-forming ability of LN metastatic tumor cells was also significantly suppressed in a dose-dependent manner by Z-GP-DAVLBH (Fig. 5G). Taken together, these data indicate that Z-GP-DAVLBH inhibits proliferation, induces apoptosis, and inhibits migration, invasion, EMT and stemness of LN metastatic tumor cells.

3.6. Z-GP-DAVLBH blocks colorectal cancer lymph node metastasis in vivo

To evaluate the effect of Z-GP-DAVLBH on CRCLNM *in vivo*, patient-derived CRCLNM xenografts were constructed, and tumor growth and lymphatic metastasis were monitored using the IVIS Lumina LT imaging system (Fig. 6A, Supporting Information Fig. S12A). Our results showed that Z-GP-DAVLBH treatment dramatically inhibited tumor growth and caused tumor regression in patient-derived CRCLNM xenografts, as indicated by the decreased number of LN metastatic niches (Fig. 6B and C). Importantly, no significant loss in body weight was observed in mice treated with Z-GP-DAVLBH (Fig. S12B). Mechanistically, Z-GP-DAVLBH suppressed tumor cell EMT, as indicated by increased E-cadherin and decreased N-cadherin and Vimentin expression, inhibited tumor stemness by decreasing the expression of CD44 and CD133, as well as suppressed tumor lymphangiogenesis by downregulating the expression of VEGFC and the number of lymphatic vessels in primary tumor tissues (Fig. 6D and E). In addition, Z-GP-DAVLBH treatment inhibited collagen I deposition and linearization in metastatic LN (Fig. 6F). These effects may be associated with Z-GP-DAVLBH-induced apoptosis in FAPα-positive LN metastatic tumor cells (Fig. 6G). Ultimately, Z-GP-DAVLBH prolonged the overall survival of mice bearing CRCLNM xenografts (from 20 to 30 days) (Fig. 6H). These data indicate that Z-GP-DAVLBH significantly induces apoptosis in LN metastatic tumor cells, suppresses tumor EMT, stemness and lymphangiogenesis, and regulates ECM, thus inhibiting CRCLNM.

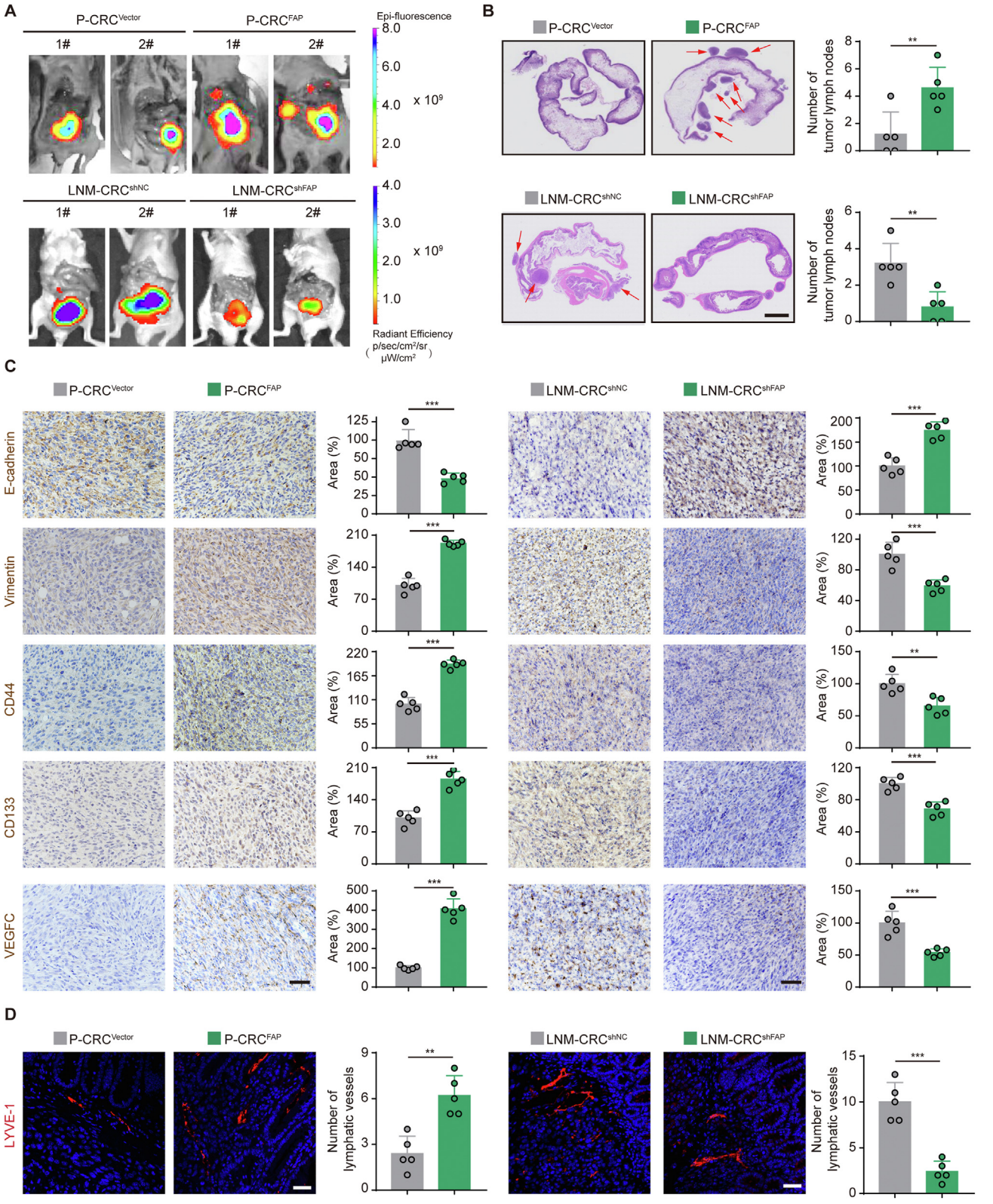

Figure 3 FAPα in tumor cells promotes colorectal cancer lymph node metastasis *in vivo*. (A) Representative images of growth and lymphatic metastasis of P-CRC^{Vector}, P-CRC^{FAP}, LNM-CRC^{shNC} and LNM-CRC^{shFAP} xenografts ($n = 5$). (B) H&E staining and quantification of the LN metastatic nodules ($n = 5$). Red arrows indicate the metastatic LN nodules. Scale bar: 2 mm. (C) Immunohistochemical staining and quantification of E-cadherin, Vimentin, CD44, CD133 and VEGFC in orthotopic tumor tissues from patient-derived CRCLNM xenografts ($n = 5$). Scale bar: 50 μm. (D) Immunofluorescence staining and quantification of LYVE-1 in orthotopic tumor tissues from patient-derived CRCLNM xenografts ($n = 5$). Scale bar, 20 μm. Data are presented as mean ± SEM. $^{**}P < 0.01$, $^{***}P < 0.001$ by two-tailed unpaired *t*-test. LNM-CRC, lymph node metastatic colorectal cancer; P-CRC, primary colorectal cancer.

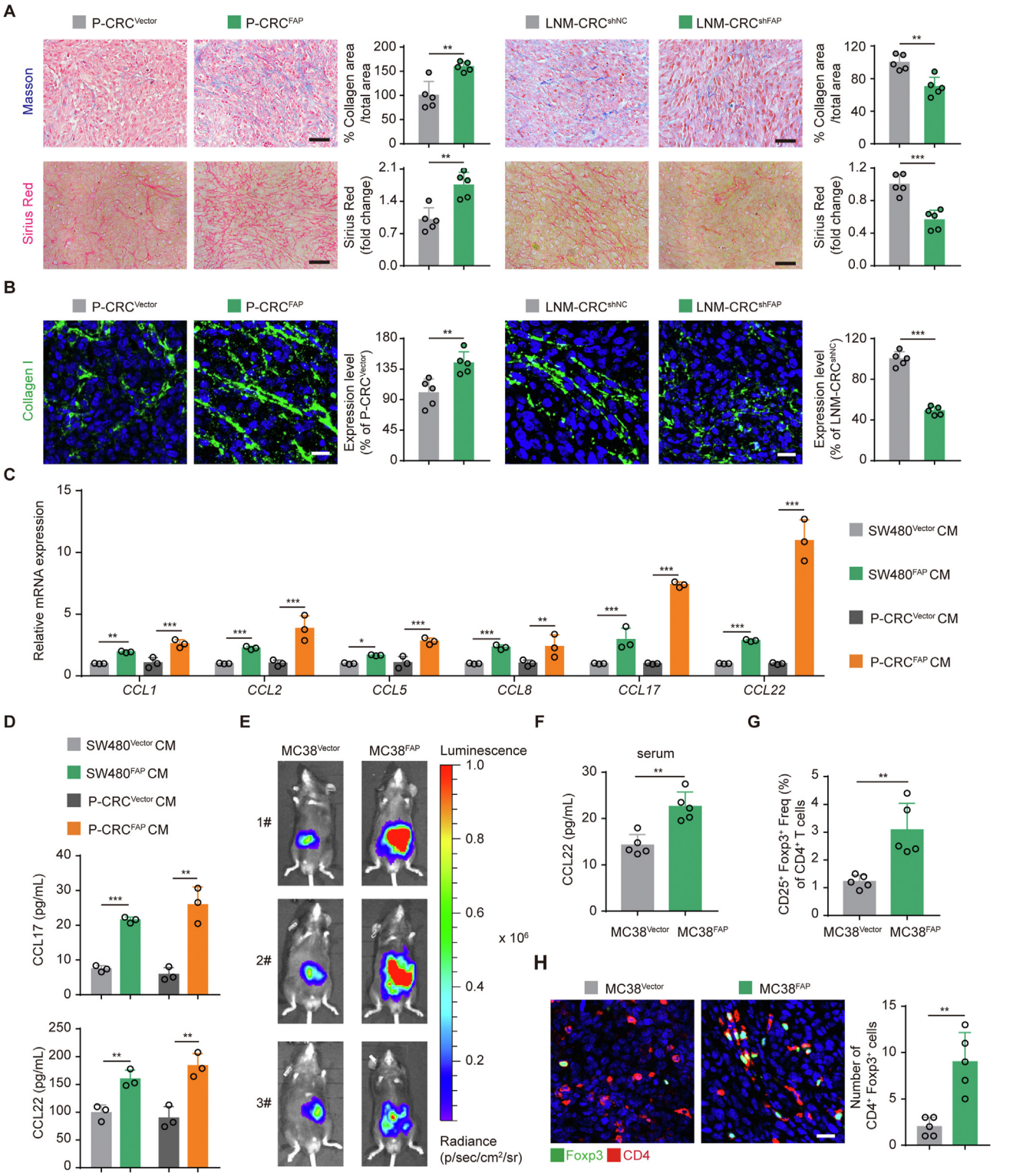

Figure 4 FAPα induces ECM remodeling and immunosuppressive environment in the metastatic lymph nodes. (A) Representative images and quantification of Masson trichrome staining and Sirius Red staining in the LN metastatic tissues from patient-derived CRCLNM xenografts ($n = 5$). Scale bar: 50 μm. (B) Immunofluorescence staining and quantification of collagen I in the LN metastatic tissues from patient-derived CRCLNM xenografts ($n = 5$). Scale bar: 20 μm. (C) RT-qPCR analysis of *CCL1*, *CCL2*, *CCL5*, *CCL8*, *CCL17* and *CCL22* levels in FAPα-overexpressing SW480 and P-CRC cells ($n = 3$). (D) Cytokine concentrations in the cell culture supernatants were measured by ELISA kit ($n = 3$). (E) Representative bioluminescence images of tumor growth and lymphatic metastasis in MC38^{Vector} and MC38^{FAP} allografts ($n = 5$). (F) Serum CCL22 levels were measured using an ELISA kit ($n = 5$). (G) Flow cytometry analysis of CD4$^+$CD25$^+$FOXP3$^+$ Treg cells in metastatic LN tissues from MC38^{Vector} and MC38^{FAP} allografts ($n = 5$). (H) Immunofluorescence staining of CD4$^+$FOXP3$^+$ Treg cells in metastatic LN tissues from MC38^{Vector} and MC38^{FAP} allografts ($n = 5$). Scale bar: 20 μm. Data are presented as mean ± SEM. $^*P < 0.05$, $^{**}P < 0.01$, $^{***}P < 0.001$ by two-tailed unpaired *t*-test. LNM-CRC, lymph node metastatic colorectal cancer; P-CRC, primary colorectal cancer.

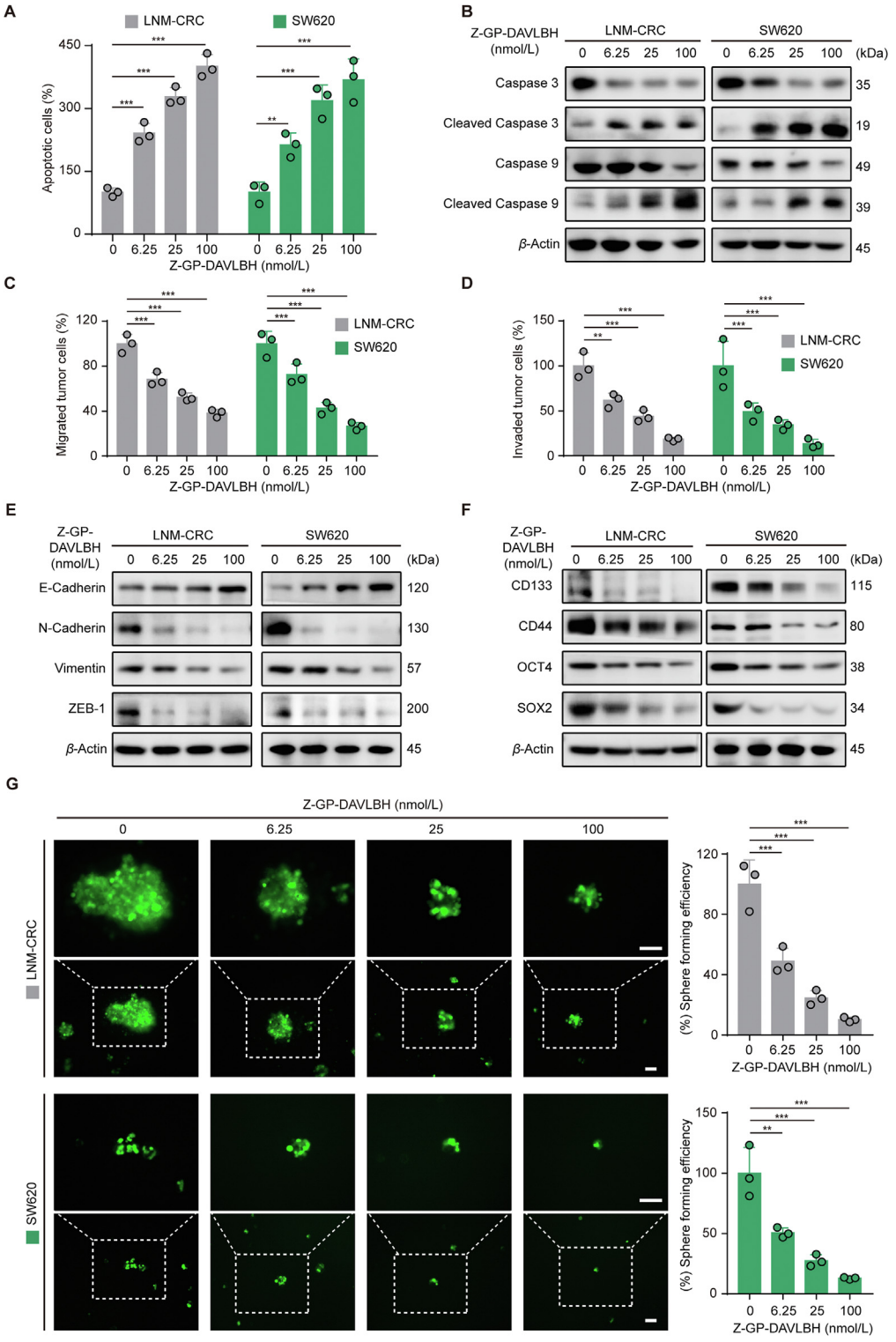

Figure 5 Z-GP-DAVLBH induces apoptosis, and inhibits the motility and stemness of the lymph node metastatic tumor cells. (A) Propidium iodide (PI) staining of LN metastatic tumor cells following Z-GP-DAVLBH treatment. Quantification of apoptotic cells is shown ($n = 3$). (B) Western blot analysis of Caspase-3, Cleaved Caspase-3, Caspase 9, and Cleaved Caspase-9 in LN metastatic tumor cells after Z-GP-DAVLBH treatment ($n = 3$). (C, D) Quantification of the number of migrated (C) and invaded (D) LN metastatic tumor cells treated with Z-GP-DAVLBH ($n = 3$). (E) Western blot analysis of the expression of E-cadherin, N-cadherin, Vimentin and ZEB-1 in LN metastatic tumor cells treated with Z-GP-DAVLBH ($n = 3$). (F) Western blot analysis of CD133, CD44, OCT-4 and SOX-2 in LN metastatic tumor cells treated with Z-GP-DAVLBH ($n = 3$). (G) Representative images and quantification of sphere-forming of LN metastatic tumor cells treated with Z-GP-DAVLBH ($n = 3$). Original magnification: 20× (top) and 10× (bottom). Scale bar: 100 μm. Data are presented as mean ± SEM. $^{**}P < 0.01$, $^{***}P < 0.001$ by one-way ANOVA followed by Tukey's *post hoc* comparison. LNM-CRC, lymph node metastatic colorectal cancer.

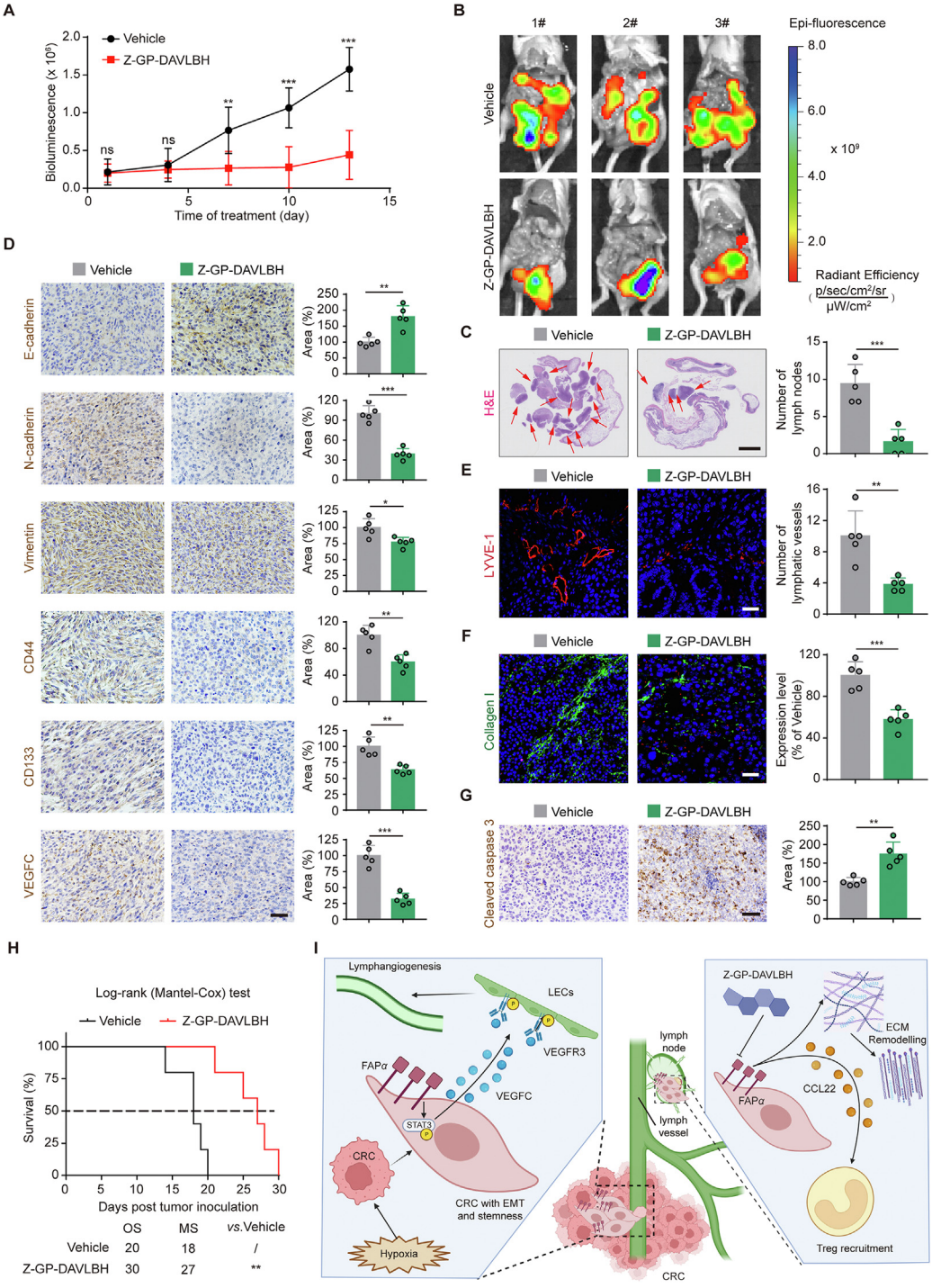

Figure 6 Z-GP-DAVLBH inhibits tumor growth and lymph node metastasis *in vivo*. (A) Quantification of bioluminescence signals in mice bearing patient-derived CRCLNM xenografts following Z-GP-DAVLBH treatment ($n = 5$). (B) Representative fluorescence images of tumor growth and lymphatic metastasis in mice bearing patient-derived CRCLNM xenografts at the endpoint of Z-GP-DAVLBH treatment ($n = 5$). (C) H&E staining and quantification of the LN metastatic nodules in mice bearing patient-derived CRCLNM xenografts after Z-GP-DAVLBH treatment ($n = 5$). Red arrows indicate the LN metastatic nodules. Scale bar: 2 mm. (D) Immunohistochemical staining and quantification of E-cadherin, N-cadherin, Vimentin, CD44, CD133 and VEGFC in orthotopic tumor tissues ($n = 5$). Scale bar: 50 μm. (E) Immunofluorescence staining and quantification of LYVE-1 in orthotopic tumor tissues ($n = 5$). Scale bar, 20 μm. (F) Immunofluorescence staining and quantification of collagen I in LN metastatic tissues ($n = 5$). Scale bar: 20 μm. (G) Immunohistochemical staining and quantification of Cleaved-caspase 3 in LN metastatic tissues ($n = 5$). Scale bar: 50 μm. (H) The overall survival (OS) curves of mice bearing patient-derived CRCLNM xenografts treated with vehicle and Z-GP-DAVLBH ($n = 5$). (I) Proposed diagram of the role of FAPα-positive LN metastatic tumor cells in CRCLNM and the therapeutic strategy. Data are presented as mean ± SEM. ns, no significance, $^*P < 0.05$, $^{**}P < 0.01$, and $^{***}P < 0.001$ (two-tailed unpaired *t*-test in A, C–G; Mantel–Cox test in H). MS, median survival; OS, overall survival.

4. Discussion

Lymphatic metastasis is one of the most typical metastatic types of malignant tumors and LN is frequently the first site of spread and growth of metastasis[34]. Since LN are widely distributed, tumor cells invading the LN have always been a substantial clinical problem in CRC therapy, whereas the underlying mechanism of metastatic tumor cells in the formation of metastatic LN has not been fully elucidated, resulting in a lack of effective therapeutic strategies targeting metastatic LN[35,36]. Here, we revealed the role of FAPα-positive tumor cells in the formation of metastatic LN and provided an effective strategy for attenuating CRCLNM. We found that tumor hypoxia induced FAPα expression in tumor cells and promoted tumor EMT, stemness, lymphangiogenesis, ECM remodeling and immune suppression, facilitating the formation of metastatic LN. Targeting FAPα-positive LNM-CRC cells by a FAPα-activated prodrug Z-GP-DAVLBH significantly inhibited CRCLNM (Fig. 6I).

The contribution of cancer cells to tumor metastasis has been well-determined[37]. However, the mechanism by which cancer cells complete the metastatic process remains unclear. Accumulating evidence reveals that the expression of specific genes is altered in metastatic tumor cells, which is essential for their adaptation and colonization of the metastatic niche[38,39]. Recently, the underlying mechanism of metastatic tumor cells contributing to the formation of metastatic LN has been revealed, and more attention has been paid to the phenotypic characteristics of metastatic tumor cells during lymphatic metastasis[5,40,41]. The phenotypic and molecular alterations in LN metastatic tumor cells are represented by acquired EMT and stemness phenotype, induced lymphangiogenesis, ECM remodeling, and an immunosuppressive microenvironment, which contribute to lymphatic metastasis[8,9,13,29,42]. Moreover, single-cell genome sequencing has recently shed light on the heterogeneity of tumor cells during lymphatic metastasis, demonstrating that the phenotypic and biological characteristics of tumor cells in the LN metastatic lesion differ from those in the primary tumor, which is being applied to discover specific therapeutic targets of LN metastatic tumor cells[9,26,43–46]. However, effective druggable targets for LN metastatic tumor cells are still lacking. Here, we focused on the properties of tumor cells in LN metastatic lesions and found that FAPα was highly expressed in LNM-CRC cells, providing a potential target for the treatment of CRCLNM.

Previous studies have identified the functional roles of FAPα in tumor migration, invasion, EMT, and stemness[20,21]. Recently, the roles of FAPα in the formation of immunosuppressive microenvironment and ECM remodeling during tumor metastasis have been highlighted[28,33,47]. LN is an important immune organ and the composition of ECM in LN is mainly collagen I[6,11], we here found that the LN metastatic tumor cells expressed FAPα, presumably to recruit immunosuppressive cells and to remodel the ECM during lymphatic metastasis. In addition, it has been demonstrated that hypoxia plays a role in lymphatic metastasis *via* the HIF-1α pathway[26,48]. However, whether hypoxia promotes lymphatic metastasis by inducing FAPα expression in tumor cells remains unclear. Here, we revealed that tumor hypoxia-induced FAPα expression in tumor cells *via* the HIF-1α pathway in a transcription-independent manner, which provided a novel insight into the mechanism underlying FAPα in tumor cells in promoting CRCLNM.

Considering the important role of FAPα in tumor progression and its restricted expression profile, it has become one of the most promising targets in tumor therapy[49]. Strategies to target FAPα-expressing cells by inhibiting its enzymatic activity include small molecule inhibitors (Identifier: NCT05420558, NCT05339113, NCT05262855, NCT04939610, NCT05432193; ClinicalTrials.gov), monoclonal antibodies (Identifier: NCT05547321, NCT00004042, NCT04826003, NCT05098405; ClinicalTrials.gov), and other immunotherapies using DNA vaccines, FAPα-directed CAR-T cells or bi-specific T cell engagers (Identifier: NCT03875079, NCT04826003, NCT03386721, NCT02627274, NCT01722149; ClinicalTrials.gov)[50]. These approaches have been evaluated in clinical trials, but most of them are unsatisfactory because of the protumorigenic effects associated with the non-enzymatic activity of FAPα[51]. Therefore, the design of peptide-based cytotoxic prodrugs based on the proteolytic activity of FAPα may be an alternative therapeutic strategy for directly killing FAPα-expressing cells. In recent years, several peptide-based cytotoxic prodrugs have been developed to target FAPα-expressing cells, showing promising effects against tumor growth[19,52]. Similarly, a FAPα-activated prodrug, Z-GP-DAVLBH, synthesized in our laboratory, exhibited potent activity against several xenograft tumors[22,23]. Our previous studies showed that Z-GP-DAVLBH can be cleaved in FAPα-positive tumor-associated mesenchymal stem cells, destroying the cells-mediated pulmonary metastasis in triple-negative breast cancer xenografts[53]. Moreover, Z-GP-DAVLBH can be activated in FAPα-positive tumor pericytes, resulting in the destruction of tumor vasculatures and inhibition of tumor growth[22]. These results highlight the effects of Z-GP-DAVLBH on tumor metastasis by targeting FAPα-positive tumor stromal cells. In the present study, considering the lack of pericyte coverage in lymphatic vessels of metastatic LN[54] and the high expression of FAPα in LNM-CRC cells, we speculated that the inhibition of CRCLNM by Z-GP-DAVLBH is primarily attributed to its targeting of FAPα-positive LNM-CRC cells. Furthermore, although some tumor cells in metastatic LN did not express FAPα, FAPα-activated prodrug may exert a marked bystander effect, which can kill those FAPα-negative tumor cells surrounding the FAPα-positive LN metastatic tumor cells[55]. Nevertheless, we cannot guarantee that Z-GP-DAVLBH completely inhibits the formation of metastatic LN, which may be supplemented by a combination with other agents.

In conclusion, our findings reveal the role of FAPα in tumor cells in CRCLNM and demonstrate that targeting FAPα-positive LNM-CRC cells may be a potential therapeutic strategy for CRCLNM.

Acknowledgments

This work was supported by the National Natural Science Foundation of China (82273941, 81973340, 82204427, 81803566, 82003796, 81773758), Local Innovative and Research Teams Project of Guangdong Pearl River Talents Program (2017BT01Y036, China), Natural Science Foundation of Guangdong Province (2022A1 515011813, 2021A1515110242, 2020A1515010071, 2019A15 15010144, 2019A1515110543, 2019A1515011934, China), Ministry of Science and Technology of China (2018ZX09711001-008-008), National high-level personnel of special support program (Zhang

Dongmei), National Key R&D Program of China (2017YFC 1703800), Technology Key Project of Guangdong Province (2020B1111110004, China), Guangdong Province Key Laboratory of Pharmacodynamic Constituents of Traditional Chinese Medicine and New Drugs Research, College of Pharmacy (2020B1212060076, China), Special Funds for the Cultivation of Guangdong College Students' Scientifc and Technological Innovation ("Climbing Program" Special Funds) (pdjh2021a0052, China), Science and Technology Projects in Guangzhou (2023A03J0602, 202201010173, 202102070001, 202002030010, China), Young S&T Talent Training Program of Guangdong Provincial Association for S&T, China (SKXRC202216), Clinical Frontier Technology Program of the First Affiliated Hospital of Jinan University (JNU1AF-CFTP-2022-a01227, China), China Postdoctoral Science Foundation (2022M 711345, China).

Author contributions

Minfeng Chen, Wencai Ye, Dongmei Zhang and Lvfen Gao designed the study. Minfeng Chen, Shuran Fan, Ming Qi and Qi Qi wrote the manuscript. Minfeng Chen, Wencai Ye, Dongmei Zhang, Lvfen Gao and Qi Qi revised the manuscript. Shuran Fan, Ming Qi, Minfeng Chen, Qun Miao, Jie Huang, Jiapeng Lin, Wenyu Lyu, Weiqing Deng, Yingyin He and Xuesong Liu carried out the experiments. Shuran Fan, Ming Qi, Minfeng Chen, Maohua Huang and Xiaobo Li performed data analysis. Qi Qi, Lijuan Deng, Jinghua Pan, Shenghui Qiu and Jiashuai He helped in experimental design and contributed materials. All authors have seen and approved the final version of the manuscript.

Conflicts of interest

The authors declare no potential conflicts of interest.

Appendix A. Supporting information

Supporting data to this article can be found online at https://doi.org/10.1016/j.apsb.2023.11.002.

References

1. Siegel RL, Miller KD, Fuchs HE, Jemal A. Cancer statistics, 2021. *CA Cancer J Clin* 2021;**71**:7−33.
2. Pereira ER, Kedrin D, Seano G, Gautier O, Meijer EFJ, Jones D, et al. Lymph node metastases can invade local blood vessels, exit the node, and colonize distant organs in mice. *Science* 2018;**359**:1403−7.
3. Biller LH, Schrag D. Diagnosis and treatment of metastatic colorectal cancer: a review. *JAMA* 2021;**325**:669−85.
4. Zhang C, Zhang L, Xu T, Xue R, Yu L, Zhu Y, et al. Mapping the spreading routes of lymphatic metastases in human colorectal cancer. *Nat Commun* 2020;**11**:1993.
5. Li YL, Hung WC. Reprogramming of sentinel lymph node microenvironment during tumor metastasis. *J Biomed Sci* 2022;**29**:84.
6. Gillot L, Baudin L, Rouaud L, Kridelka F, Noel A. The pre-metastatic niche in lymph nodes: formation and characteristics. *Cell Mol Life Sci* 2021;**78**:5987−6002.
7. Karaman S, Detmar M. Mechanisms of lymphatic metastasis. *J Clin Investig* 2014;**124**:922−8.
8. Karlsson MC, Gonzalez SF, Welin J, Fuxe J. Epithelial−mesenchymal transition in cancer metastasis through the lymphatic system. *Mol Oncol* 2017;**11**:781−91.
9. Xu K, Wang R, Xie H, Hu L, Wang C, Xu J, et al. Single-cell RNA sequencing reveals cell heterogeneity and transcriptome profile of breast cancer lymph node metastasis. *Oncogenesis* 2021;**10**:66.
10. Das S, Sarrou E, Podgrabinska S, Cassella M, Mungamuri SK, Feirt N, et al. Tumor cell entry into the lymph node is controlled by CCL1 chemokine expressed by lymph node lymphatic sinuses. *J Exp Med* 2013;**210**:1509−28.
11. Li X, Zhao J, Kasinath V, Uehara M, Jiang L, Banouni N, et al. Lymph node fibroblastic reticular cells deposit fibrosis-associated collagen following organ transplantation. *J Clin Investig* 2020;**130**:4182−94.
12. Winkler J, Abisoye-Ogunniyan A, Metcalf KJ, Werb Z. Concepts of extracellular matrix remodelling in tumour progression and metastasis. *Nat Commun* 2020;**11**:5120.
13. Reticker-Flynn NE, Zhang W, Belk JA, Basto PA, Escalante NK, Pilarowski GOW, et al. Lymph node colonization induces tumor-immune tolerance to promote distant metastasis. *Cell* 2022;**185**:1924−1942.e23.
14. Lund AW. Lymph node metastasis: an immunological burden. *J Exp Med* 2023;**220**:e20230904.
15. Liu S, Chen X, Lin T. Lymphatic metastasis of bladder cancer: molecular mechanisms, diagnosis and targeted therapy. *Cancer Lett* 2021;**505**:13−23.
16. Duan H, Liu Y, Gao Z, Huang W. Recent advances in drug delivery systems for targeting cancer stem cells. *Acta Pharm Sin B* 2021;**11**:55−70.
17. Aertgeerts K, Levin I, Shi L, Snell GP, Jennings A, Prasad GS, et al. Structural and kinetic analysis of the substrate specificity of human fibroblast activation protein alpha. *J Biol Chem* 2005;**280**:19441−4.
18. Pure E, Blomberg R. Pro-tumorigenic roles of fibroblast activation protein in cancer: back to the basics. *Oncogene* 2018;**37**:4343−57.
19. Brennen WN, Rosen DM, Wang H, Isaacs JT, Denmeade SR. Targeting carcinoma-associated fibroblasts within the tumor stroma with a fibroblast activation protein-activated prodrug. *J Natl Cancer Inst* 2012;**104**:1320−34.
20. Cao F, Wang S, Wang H, Tang W. Fibroblast activation protein-α in tumor cells promotes colorectal cancer angiogenesis *via* the Akt and ERK signaling pathways. *Mol Med Rep* 2018;**17**:2593−9.
21. Yuan Z, Hu H, Zhu Y, Zhang W, Fang Q, Qiao T, et al. Colorectal cancer cell intrinsic fibroblast activation protein alpha binds to Enolase1 and activates NF-κB pathway to promote metastasis. *Cell Death Dis* 2021;**12**:543.
22. Chen M, Lei X, Shi C, Huang M, Li X, Wu B, et al. Pericyte-targeting prodrug overcomes tumor resistance to vascular disrupting agents. *J Clin Investig* 2017;**127**:3689−701.
23. Qi M, Fan S, Huang M, Pan J, Li Y, Miao Q, et al. Targeting FAPα-expressing hepatic stellate cells overcomes resistance to anti-angiogenics in colorectal cancer liver metastasis models. *J Clin Investig* 2022;**132**:e157399.
24. Ye G, Huang M, Li Y, Ouyang J, Chen M, Wen Q, et al. The FAPα-activated prodrug Z-GP-DAVLBH inhibits the growth and pulmonary metastasis of osteosarcoma cells by suppressing the AXL pathway. *Acta Pharm Sin B* 2022;**12**:1288−304.
25. Cespedes MV, Espina C, Garcia-Cabezas MA, Trias M, Boluda A, Gomez del Pulgar MT, et al. Orthotopic microinjection of human colon cancer cells in nude mice induces tumor foci in all clinically relevant metastatic sites. *Am J Pathol* 2007;**170**:1077−85.
26. Qian Y, Zhai E, Chen S, Liu Y, Ma Y, Chen J, et al. Single-cell RNA-seq dissecting heterogeneity of tumor cells and comprehensive dynamics in tumor microenvironment during lymph nodes metastasis in gastric cancer. *Int J Cancer* 2022;**151**:1367−81.
27. Wang H, Wu Q, Liu Z, Luo X, Fan Y, Liu Y, et al. Downregulation of FAP suppresses cell proliferation and metastasis through PTEN/PI3K/AKT and Ras-ERK signaling in oral squamous cell carcinoma. *Cell Death Dis* 2014;**5**:e1155.
28. Yang X, Lin Y, Shi Y, Li B, Liu W, Yin W, et al. FAP promotes immunosuppression by cancer-associated fibroblasts in the tumor

microenvironment *via* STAT3−CCL2 signaling. *Cancer Res* 2016;**76**:4124−35.
29. Stacker SA, Achen MG, Jussila L, Baldwin ME, Alitalo K. Lymphangiogenesis and cancer metastasis. *Nat Rev Cancer* 2002;**2**:573−83.
30. Huang YH, Yang HY, Huang SW, Ou G, Hsu YF, Hsu MJ. Interleukin-6 induces vascular endothelial growth factor-C expression *via* Src−FAK−STAT3 signaling in lymphatic endothelial cells. *PLoS One* 2016;**11**:e0158839.
31. Tammela T, Alitalo K. Lymphangiogenesis: molecular mechanisms and future promise. *Cell* 2010;**140**:460−76.
32. Provenzano PP, Eliceiri KW, Campbell JM, Inman DR, White JG, Keely PJ. Collagen reorganization at the tumor-stromal interface facilitates local invasion. *BMC Med* 2006;**4**:38.
33. Lee HO, Mullins SR, Franco-Barraza J, Valianou M, Cukierman E, Cheng JD. FAP-overexpressing fibroblasts produce an extracellular matrix that enhances invasive velocity and directionality of pancreatic cancer cells. *BMC Cancer* 2011;**11**:245.
34. Nathanson SD, Shah R, Rosso K. Sentinel lymph node metastases in cancer: causes, detection and their role in disease progression. *Semin Cell Dev Biol* 2015;**38**:106−16.
35. Jones D, Pereira ER, Padera TP. Growth and immune evasion of lymph node metastasis. *Front Oncol* 2018;**8**:36.
36. Royston D, Jackson DG. Mechanisms of lymphatic metastasis in human colorectal adenocarcinoma. *J Pathol* 2009;**217**:608−19.
37. Chambers AF, Groom AC, MacDonald IC. Dissemination and growth of cancer cells in metastatic sites. *Nat Rev Cancer* 2002;**2**:563−72.
38. Ganesh K, Massague J. Targeting metastatic cancer. *Nat Med* 2021;**27**:34−44.
39. Huang D, Sun W, Zhou Y, Li P, Chen F, Chen H, et al. Mutations of key driver genes in colorectal cancer progression and metastasis. *Cancer Metastasis Rev* 2018;**37**:173−87.
40. Pereira ER, Jones D, Jung K, Padera TP. The lymph node microenvironment and its role in the progression of metastatic cancer. *Semin Cell Dev Biol* 2015;**38**:98−105.
41. Mohammed SI, Torres-Luquis O, Walls E, Lloyd F. Lymph-circulating tumor cells show distinct properties to blood-circulating tumor cells and are efficient metastatic precursors. *Mol Oncol* 2019;**13**:1400−18.
42. Hoshida T, Isaka N, Hagendoorn J, di Tomaso E, Chen YL, Pytowski B, et al. Imaging steps of lymphatic metastasis reveals that vascular endothelial growth factor-C increases metastasis by increasing delivery of cancer cells to lymph nodes: therapeutic implications. *Cancer Res* 2006;**66**:8065−75.
43. Wang B, Zhang Y, Qing T, Xing K, Li J, Zhen T, et al. Comprehensive analysis of metastatic gastric cancer tumour cells using single-cell RNA-seq. *Sci Rep* 2021;**11**:1141.
44. Palmieri V, Lucchetti D, Maiorana A, Papi M, Maulucci G, Calapa F, et al. Mechanical and structural comparison between primary tumor and lymph node metastasis cells in colorectal cancer. *Soft Matter* 2015;**11**:5719−26.
45. Meacham CE, Morrison SJ. Tumour heterogeneity and cancer cell plasticity. *Nature* 2013;**501**:328−37.
46. Lei Y, Tang R, Xu J, Wang W, Zhang B, Liu J, et al. Applications of single-cell sequencing in cancer research: progress and perspectives. *J Hematol Oncol* 2021;**14**:91.
47. Mazur A, Holthoff E, Vadali S, Kelly T, Post SR. Cleavage of type I collagen by fibroblast activation protein-alpha enhances class A scavenger receptor mediated macrophage adhesion. *PLoS One* 2016;**11**:e0150287.
48. Rofstad EK, Rasmussen H, Galappathi K, Mathiesen B, Nilsen K, Graff BA. Hypoxia promotes lymph node metastasis in human melanoma xenografts by up-regulating the urokinase-type plasminogen activator receptor. *Cancer Res* 2002;**62**:1847−53.
49. Zhao L, Chen J, Pang Y, Fu K, Shang Q, Wu H, et al. Fibroblast activation protein-based theranostics in cancer research: a state-of-the-art review. *Theranostics* 2022;**12**:1557−69.
50. Chen X, Song E. Turning foes to friends: targeting cancer-associated fibroblasts. *Nat Rev Drug Discov* 2019;**18**:99−115.
51. Juillerat-Jeanneret L, Tafelmeyer P, Golshayan D. Fibroblast activation protein-α in fibrogenic disorders and cancer: more than a prolyl-specific peptidase?. *Expert Opin Ther Targets* 2017;**21**:977−91.
52. Huang S, Fang R, Xu J, Qiu S, Zhang H, Du J, et al. Evaluation of the tumor targeting of a FAPα-based doxorubicin prodrug. *J Drug Target* 2011;**19**:487−96.
53. Li X, Chen M, Lu W, Tang J, Deng L, Wen Q, et al. Targeting FAPα-expressing tumor-associated mesenchymal stromal cells inhibits triple-negative breast cancer pulmonary metastasis. *Cancer Lett* 2021;**503**:32−42.
54. Zwaans BM, Bielenberg DR. Potential therapeutic strategies for lymphatic metastasis. *Microvasc Res* 2007;**74**:145−58.
55. Kim MG, Shon Y, Kim J, Oh YK. Selective activation of anticancer chemotherapy by cancer-associated fibroblasts in the tumor microenvironment. *J Natl Cancer Inst* 2017;**109**:djw186.